Chinese Chemical Letters 34 (2023) 108310

Contents lists available at ScienceDirect

Chinese Chemical Letters

journal homepage: www.elsevier.com/locate/cclet

Enhancing the singlet oxygen capture and release rate of metal–organic frameworks through interpenetration tuning

Jing Hao[a], Feifan Lang[b], Liqin Hao[a], Yi Yang[a], Lulu Zhang[a], Hao Zhang[b], Quan-Wen Li[b], Jiandong Pang[b,c,*], Xian-He Bu[a,b,c,*]

[a] College of Chemistry, State Key Laboratory of Elemento-Organic Chemistry, Nankai University, Tianjin 300071, China
[b] School of Materials Science and Engineering, Smart Sensing Interdisciplinary Science Center, Tianjin Key Laboratory of Metal and Molecule-Based Material Chemistry, Nankai University, Tianjin 300350, China
[c] Haihe Laboratory of Sustainable Chemical Transformations, Tianjin 300192, China

ARTICLE INFO

Article history:
Received 24 December 2022
Revised 17 January 2023
Accepted 6 March 2023
Available online 15 March 2023

Keywords:
Metal-organic framework
Singlet oxygen capture and release
Regulation
Single-crystal to single-crystal transformation
Anti-fake application

ABSTRACT

Recognized as one of the important active species involved in various reactions, singlet oxygen ($^1O_2$) shows potential applications in chemical, biological, and environmental related fields. However, the controlled capture and release of $^1O_2$ are still facing huge challenges due to its short lifetime and high reactivity. Herein, a framework-interpenetration tuning strategy was applied on a metal-organic framework (MOF) that aiming to improve the capture and release rate of $^1O_2$. The porosity of the MOF was remarkably enhanced with the structural evolution from seven-fold (termed NKM-181) to six-fold interpenetration (termed NKM-182), and the active anthracene sites became much more accessible. Such drastic process can be achieved as simple as exchanging the primitive MOF in selected solvent and occurred surprisingly as single-crystal to single-crystal transformation. Also, additionally owing to the unblocked regular channels, NKM-182 shown significantly improved $^1O_2$ trapping and releasing rates compared to that of in NKM-181. This work demonstrates an unprecedented regulation of $^1O_2$ capture and release process, along with achieving the highest $^1O_2$ capture and release rate among reported porous materials. Furthermore, the obtained endoperoxides with $^1O_2$ loaded (termed EPO-NKM-181 and EPO-NKM-182) can be used as a high efficiency smart material for anti-fake application

Singlet oxygen ($^1O_2$) is an excited state of molecular oxygen, which can be obtained *via* chemical reactions, cellular metabolisms, or photoexcitation of ground-state oxygen [1,2]. The controlled capture and release of $^1O_2$ is of great significance owing to its potential applications in industrial wastewater treatment, photochemical organic synthesis, photodynamic therapy, and so on [3–6]. It has been confirmed that some specific aromatic derivatives able to capture $^1O_2$ through endo-peroxidation reaction (endo-peroxidation reaction is the [4 + 2] cycloaddition reaction of forming endoperoxides from singlet oxygen and possibly canthracene, pyridone, or naphthalene.) with $^1O_2$ to form endoperoxides (EPOs) and release it under external thermal stimulation or ultraviolet irradiation [7]. In which, most of the compounds capable in such process were functionalized with anthracene, 2-pyridinone, or naphthalene [8–10]. However, the reported aromatic compounds usually show low $^1O_2$ capture and release efficiency due to their poor solubility, amorphous aggregation, and non-porous structures in general, which lead to the inaccessibility of the active sites [10]. In addition, many EPOs based on polycyclic aromatic hydrocarbons are unstable under ambient conditions and exhibit poor recyclability, which seriously affects their applications [3]. Besides, the precise regulation of $^1O_2$ capture and release rates is of great importance for achieving practical applications due to its short lifetime and high reactivity, which so far has not been perfectly solved [11]. Therefore, it is urgently needed to construct new porous materials with regular functional channels, high stability, and good recyclability, in order to further achieve accurate regulation of the trapping and releasing rate of $^1O_2$.

Due to their highly tunable pore structures and definite structural-property relationships, metal-organic frameworks (MOFs) or porous coordination polymers (PCPs) have attracted widely attentions, and show potential applications in gas adsorption and separation [12–16], chemical sensing, drug delivery, and catalysis [17–24]. With the development of crystal engineering, the

* Corresponding authors.
E-mail addresses: jdpang@nankai.edu.cn (J. Pang), buxh@nankai.edu.cn (X.-H. Bu).

https://doi.org/10.1016/j.cclet.2023.108310
1001-8417/

structures of MOFs can be predesigned and predicted according to several useful strategies such as reticular chemistry and soft/hard acid/base principle [25–29]. In addition, the pore environment of the as-synthesized MOFs can be precisely tuned by post-synthetic modification, including metal/linker exchange or installation [30–32]. Therefore, MOFs with various as-designed functions can be obtained.

Many pioneering works have confirmed that MOFs constructed from anthracene-based linkers can capture $^1O_2$ through cycloaddition reactions to form EPOs, which exhibit excellent $^1O_2$ release properties under heating or ultraviolet (UV) irradiation [33–35]. For example, a two-fold interpenetrating MOF based on the anthracene-containing DPA linker was reported by Matsuda and co-workers, which reacts with $^1O_2$ and produces anthracene endoperoxide proved by crystallographic data. Quantitatively reverse reaction proceeds under heat and the material can be used for the removal of gaseous oxygen in water under ppm level [36]. However, the regulation of $^1O_2$ capture and release rates by structural switching in MOFs has been rarely reported. We believe that the varied post-synthetic methods can bring new opportunities to the $^1O_2$ capture and release property tuning of MOFs [22,37,38]. Based on the previous research, we demonstrated that single-crystal to single-crystal structural transformation of an anthracene-based MOF (NKM-181, "NKM" stands for School of Materials Science and Engineering, Nankai University) from seven-fold to six-fold interpenetration (NKM-182) can be achieved by post-synthetic modification under the assisted of solvent, showing an increased porosity and more accessible active anthracene sites, which led to a dramatically enhanced $^1O_2$ capture and release efficiency.

The anthracene derivative 9,10-di(pyridin-4-yl)anthracene (DPA) and the elongated ditopic carboxylic linker 2′,5′-bis(trifluoromethyl)-[1,1′:4′,1″-terphenyl]-4,4″-dicarboxylic acid (H_2TPDC-2CF_3) were selected to prepare the $^1O_2$ trapping MOFs. Due to the poor solubility of the elongated ditopic carboxylic linker, we introduced -CF_3 groups to improve both the solubility of ligand and the stability of the MOFs. NKM-181 can be synthesized by reaction of DPA, H_2TPDC-2CF_3 with $Cd(NO_3)_2{\cdot}4H_2O$ in DMF, EtOH and H_2O for 72 h at 100 °C, and NKM-182 can be obtained after soaking NKM-181 in methanol for 4 h under ambient temperature (Fig. 1). Single-crystal X-ray analysis revealed that NKM-181 crystallizes in the monoclinic space group *C*2/*c* and the asymmetric unit consists of one Cd^{2+} ion, one TPDC-2CF_3^{2-} fragment, one DPA ligand, and one coordinated H_2O molecule. The Cd^{2+} ion is coordinated in a trigonal-bipyramidal geometry defined by two pyridyl nitrogen atoms of two DPA ligands, two carboxylate oxygen atoms from two TPDC-2CF_3^{2-} fragments and one oxygen atom from the coordinated H_2O molecule. Each TPDC-2CF_3^{2-} fragment links to two independent Cd^{2+} ions *via* two oxygen atoms from two carboxyl groups, and each DPA ligand coordinates to two Cd^{2+} ions *via* two pyridyl donors. On the whole, a three-dimensional framework with quadrilateral pores was formed, which can be descripted as a **dia** topology framework with the Cd^{2+} ions simplified as 4-connected nodes. Such **dia** framework consists with large quadrilateral pores but are filled *via* mutual interpenetration to another six of its equivalents into an overall seven-fold 3D network with no potentially accessible voids determined. Different from that of NKM-181, NKM-182 crystallizes in the monoclinic space group *P*2/*c* and the asymmetric unit consists of one Cd^{2+} ion, one TPDC-2CF_3^{2-} fragment and one DPA ligand. The Cd^{2+} ion is coordinated in a twisted octahedral geometry defined by two pyridyl nitrogen atoms from two DPA ligands and four carboxyl oxygen atoms from two TPDC-2CF_3^{2-} fragments. The carboxyl oxygen atom on each TPDC-2CF_3^{2-} fragment binds to two independent Cd^{2+} ions in a bidentate chelated coordination fashion, and each DPA ligand coordinates to two Cd^{2+} ions *via* two pyridyl groups (Figs. S1 and S2 in Supporting information). Interestingly, the terminal coordinated water molecules observed in NKM-181 were removed through methanol soaking (no coordinated methanol observed). Similar **dia** topological networks can be obtained if the Cd^{2+} ion was simplified as 4-connected nodes. The size of the quadrilateral channel in a single framework of NKM-182 is slightly smaller than that of in NKM-181 due to the increased steric hindrance from the anthracene groups that are now oriented more orthogonal to the channels. A six-fold interpenetrated network, rather than seven-fold, was formed in NKM-182 with preserved rectangular open channels (dimensions of approximately 9.17 Å × 14.29 Å). The active anthracene sites are therefore more exposed than those of in NKM-181, which possibly dominating the significant increase in $^1O_2$ capture and release rates.

The robustness of two MOFs was tested before $^1O_2$ trapping measurements, and both of NKM-181 and NKM-182 show good

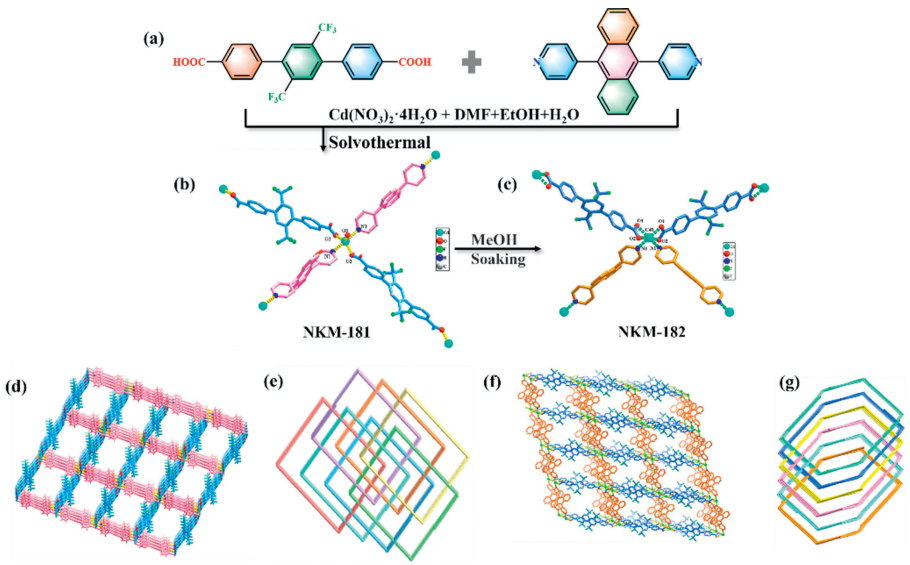

Fig. 1. Synthesis and structural description of NKM-181 and NKM-182: (a) The synthesis of NKM-181; (b, c) Coordination modes of the Cd^{2+} ions in NKM-181 and NKM-182; (d, f) The **dia** topological networks in NKM-181 and NKM-182; (e, g) The seven-fold and six-fold interpenetration frameworks in NKM-181 and NKM-182.

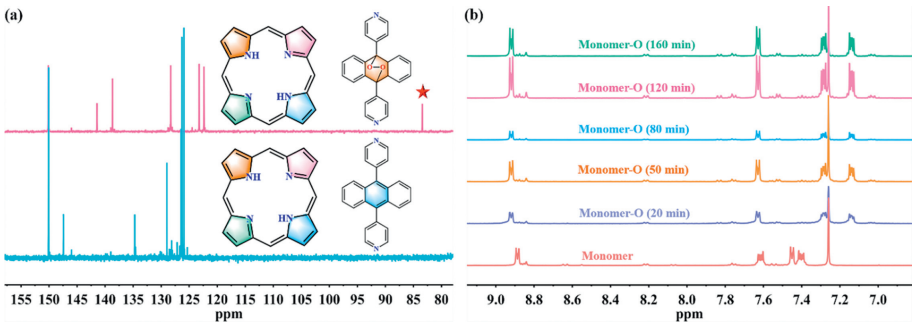

Fig. 2. (a) ^{13}C NMR spectra of DPA before (blue) and after (pink) photo-oxygenation (star peak represents peroxidation bonds). (b) Time resolved ^{1}H NMR spectra of the $^{1}O_2$ capturing by DPA.

thermal and chemical stabilities. Combination of thermogravimetric analysis curves and temperature-variable PXRD patterns confirmed that NKM-181 and NKM-182 are very stable until reached ~320 °C and ~360 °C, respectively (Figs. S3 and S4 in Supporting information). The chemical stability of the MOFs was investigated by immersing crystalline samples in aqueous solutions with pH ranging between 2 and 12 or various solvents. The PXRD patterns proved that both two frameworks remained intact after treated in weak acidic or basic solution (pH 4-12, Fig. S5 in Supporting information), or in common types of organic solvents apart from the combination of NKM-181/methanol (Fig. S6 in Supporting information). A drastic single-crystal-to-single-crystal phase transition occurred from NKM-181 (seven-fold interpenetration) to NKM-182 (six-fold interpenetration) when immersing the former into methanol. Therefore, the PXRD patterns remarkably changed for the methanol treated NKM-181, which is now consistent with the simulated ones for NKM-182.

In order to verify whether NKM-181 and NKM-182 can effectively capture and release of $^{1}O_2$, we prepared EPO-DPA by [4 + 2]-cycloaddition of DPA and $^{1}O_2$ under 660 nm light-emitting diode (LED) irradiation using 5,10,15,20-tetraphenylporphyrin (TPP) as the photosensitizing agent. As shown in Fig. 2a, a new peak centered at 84 ppm appeared on the ^{13}C NMR spectrum of EPO-DPA, which can be attributed to the formation of peroxidation bonds in EPO-DPA. Time resolved ^{1}H NMR spectrum was used to trace the trapping process of $^{1}O_2$. As shown in Fig. 2b, a new peak centered at 7.1 ppm appeared on the ^{1}H NMR spectrum after 20 min, indicating the generation of EPO-DPA. The electrospray ionization mass spectrometry (ESI-MS) data of EPO-DPA showed the *quasi*-molecular ion peak at mass-to-charge ratio (*m/z*) of 365.1, indicating the successfully capture of $^{1}O_2$ by the DPA linkers (Fig. S7 in Supporting information).

Fluorescence spectroscopic measurements were used to demonstrate the successfully capture and release of $^{1}O_2$ by the MOFs. 5 mg NKM-181 or NKM-182, 0.5 mg meso–tetraphenylporphyrin (TPP) and 20 mL DMF were added to a round-bottom flask and treated with ultrasound in an ice bath for 20 min to give a purple suspension. The mixture was then illuminated by light of a wavelength 660 nm under pure oxygen flow, before fluorescence spectra were collected at different reaction times. As expected, NKM-181 and NKM-182 behave similar during $^{1}O_2$ trapping, thus NKM-182 will be discussed in detail as a representative for brevity. As shown in Fig. 3a, the fluorescence peak intensity of NKM-182 gradually decreased with the increase of irradiation time and hardly show

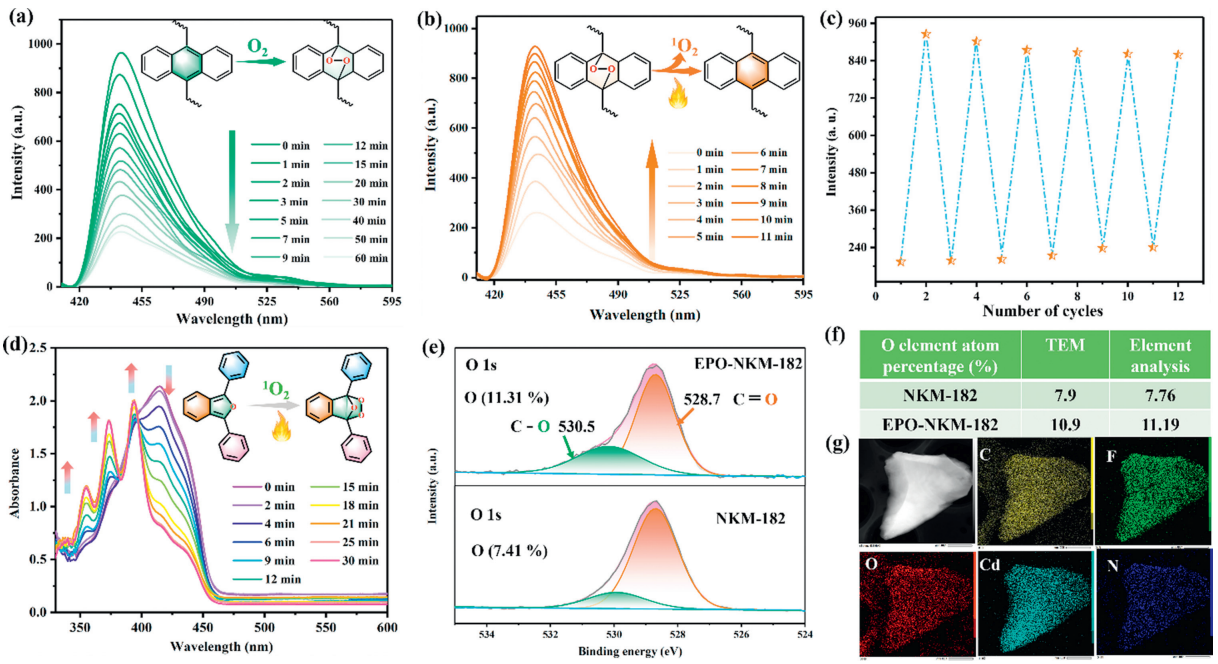

O element atom percentage (%)	TEM	Element analysis
NKM-182	7.9	7.76
EPO-NKM-182	10.9	11.19

Fig. 3. (a) Time resolved fluorescence spectra of NKM-182 in the process of $^{1}O_2$ capturing and (b) releasing under heat. (c) Fluorescence intensities of NKM-182 in multiple cycles of $^{1}O_2$ capture and thermal triggered release. (d) Time resolved UV–vis absorption spectra of 1,3-diphenylisobenzofuran in DMF at 373 K in the presence of EPO-NKM-182. (e) XPS spectra of NKM-182 and EPO-NKM-182 (O 1 s) (7.41% and 11.31% represented for the O element atom percentage of NKM-182 and EPO-NKM-182). (f) Oxygen elemental contents of NKM-182 and EPO-NKM-182. (g) TEM image and EDX elemental mapping of NKM-182.

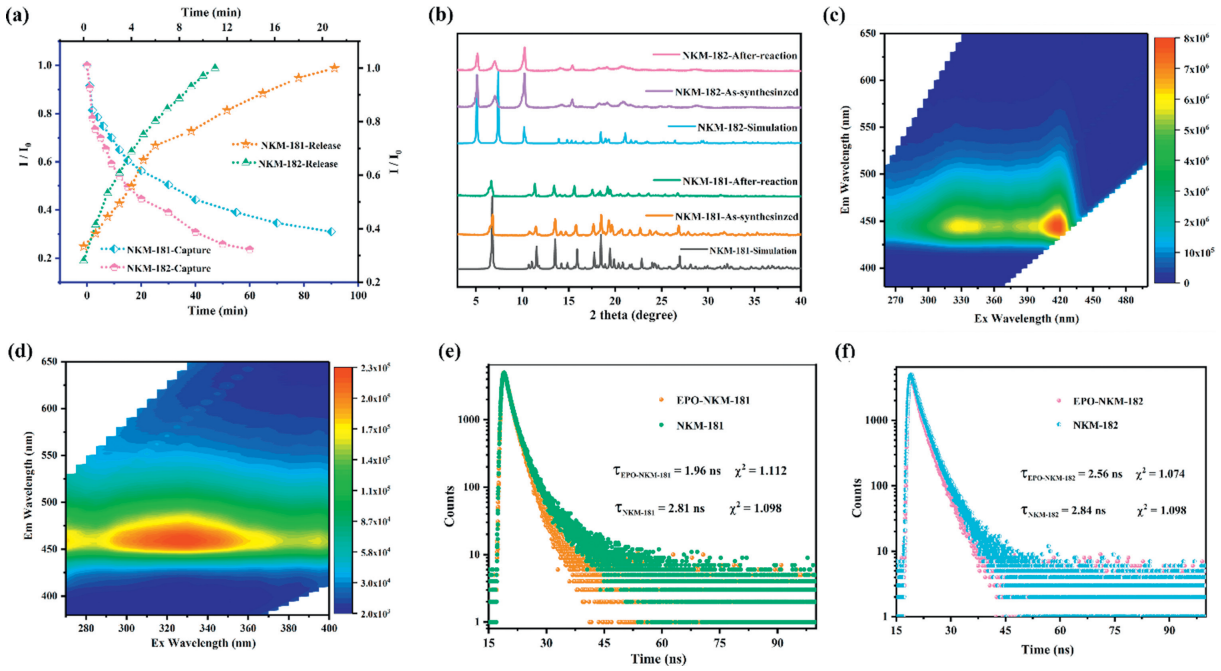

Fig. 4. (a) Comparison of NKM-181 and NKM-182 for $^1O_2$ trapping rates and thermal triggered releasing rates (blue axes: capture; black axes: release). (b) PXRD patterns of NKM-181 and NKM-182, pre- and after-reaction and simulated. Solid-state fluorescence excitation-emission matrix spectra of (c) NKM-181 and (d) NKM-182. Fluorescence decay profiles of (e) NKM-181 and (f) NKM-182.

further changes after about 60 min of reaction, indicating the continuous formation of the endoperoxides EPO-NKM-182 before the saturation of the reaction between anthracene group and $^1O_2$.

Then the photodegradation reaction of EPO-NKM-182, *i.e.*, the release of the $^1O_2$ from the endoperoxides, was also carefully investigated. According to the literature, the photocycloreversion reaction of endoperoxide derivatives occurred in the upper excited singlet state π-π^*, while the decomposition reaction was taken place in the lowest excited state S1 ($\pi^*\sigma^*$), corresponding to the partly excited peroxide chromophore [7]. There are two absorption bands in the UV–vis spectrum of EPO-NKM-182, containing a high-energy absorption at ~265 nm and low-energy absorptions that exceed 290 nm (Fig. S8 in Supporting information). Therefore, the 254 nm light was chosen to trigger the decomposition reaction of EPO-NKM-182, and time resolved fluorescence spectrum was recorded to track the reaction process. The fluorescence intensity increased with the irradiation time extended, and the reaction basically completed in about 30 min (Fig. S9 in Supporting information). In addition to light irradiation, heating is another commonly used method to initiate the endoperoxide decomposition reaction. Upon heating at 100 °C, the weakened fluorescence intensity of EPO-NKM-182 gradually raise back, and almost restored as of before capture within only 11 min (Fig. 3b). The $^1O_2$ capture and release processes of NKM-182 are reversible and can tolerate at least six cycles without significant decrease of the loading amount (Fig. 3c). To verify the oxygen released from the system was under excited state, 1,3-diphenylisobenzofuran and EPO-NKM-182 were dispersed into 20 mL of DMF and heated at 100 °C, and the characteristic absorption of 1,3-diphenylisobenzofuran at 410 nm decreased in the UV–vis absorption spectra, revealing the release of $^1O_2$ from EPO-NKM-182 (Fig. 3d). Additionally, the X-ray photoelectron spectroscopy (XPS), transmission electron microscopy (TEM), elemental analysis (EA), and scanning electron microscope (SEM) results displayed that the content of oxygen in EPO-NKM-182 increased after binding $^1O_2$, which proves that $^1O_2$ has been successfully captured (Figs. 3e-g and Figs. S10-S13 in Supporting information).

The ratio of the fluorescence intensity to the original fluorescence intensity (I/I_0) of NKM-181 and NKM-182 were used to further evaluate the $^1O_2$ trapping and releasing efficiency. As shown in Fig. 4a and Table S3 (Supporting information), the rate of $^1O_2$ trapping and releasing for NKM-182 is much faster than that of NKM-181. The PXRD studies indicated that the structural integrity of NKM-181 and NKM-182 were fully retained after the completion of six reaction cycles (Fig. 4b). The fluorescence emission peak under solid state remained at 445 nm when the excitation wavelength increased from 320 nm to 420 nm in the three-dimensional fluorescence spectrogram of NKM-181 (Fig. 4c). The excitation wavelength of NKM-182 ranges from 290 nm to 370 nm, but the position of the fluorescence emission peak is consistent with that of NKM-181 (Fig. 4d). Therefore, the delayed fluorescence spectra at 445 nm before and after $^1O_2$ capture of both MOFs were tested. As shown in Figs. 4e and f, the fluorescence lifetime for both compounds were all weakened after binding $^1O_2$, as a consequence of destroyed conjugated structure after trapping $^1O_2$. Compared with NKM-181, the efficiency of trapping and releasing $^1O_2$ of NKM-182 is significantly improved under the same test conditions (Figs. S14-S19 in Supporting information).

The single-crystal structures of NKM-181 and NKM-182 were carefully analysed in order to figure out the reason for the improvement of the $^1O_2$ trapping and release properties. As shown in Fig. 5a, NKM-181 is a densely packed structure without solvent accessible voids, while open channels with dimensions of approximately 9.17 Å × 14.29 Å can be observed in NKM-182. Therefore, we infer that the regular pores in NKM-182 can be beneficial to the transfer of $^1O_2$ in the MOFs. Furthermore, the EPO-NKM-181 and EPO-NKM-182 can be used as smart materials for anti-fake applications. The EPO-NKM-181 (Fig. S21 in Supporting information) or EPO-NKM-182 (Fig. 5b) powder was sprinkled on a glass substrate with the shape of "181" or "182" characters and irradiated with 365 nm light to emit a weak fluorescence. The intensity of the blue fluorescence for "181" and "182" remarkably increased after heated the glass at 100 °C, which was due to the release of the captured $^1O_2$.

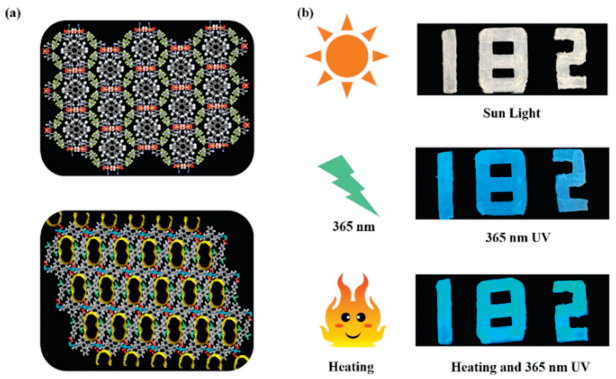

Fig. 5. (a) The three-dimensional structures of NKM-181 (top) and NKM-182 (bottom) packed by Mercury software. (b) The images of EPO-NKM-182 under sunlight, 365 nm irradiation and heating.

In conclusion, interpenetration tuning of the anthracene-based MOFs from seven-fold (NKM-181) to six-fold (NKM-182) have been successfully achieved through solvent assisted single-crystal to single-crystal transformation. Both NKM-181 and NKM-182 present good thermal and chemical stability, with $^1O_2$ capture and release properties proved and investigated from multiple perspectives. Compared to NKM-181, NKM-182 shows increased structural porosity, better accessible active anthracene sites, and enhanced $^1O_2$ capture and release efficiency. In addition, the prepared endoperoxides EPD-NKM-181 and EPD-NKM-182 exhibit attractive potential for anti-fake purpose. This work provides a new platform for $^1O_2$ capture, storage, and related promising applications.

Declaration of competing interest

The authors declare that they have no known competing financial interest or personal relationships that could have appeared to influence the work reported in this paper.

Acknowledgments

The authors acknowledge the financial support of the National Natural Science Foundation of China (Nos. 22035003 and 22201137), Nature Science Fund of Tianjin, China (No. 19JCZDJC37200), Fundamental Research Funds for the Central Universities (No. 63223020) and the Haihe Laboratory of Sustainable Chemical Transformations (No. YYJC202101).

Supplementary materials

Supplementary material associated with this article can be found, in the online version, at doi:10.1016/j.cclet.2023.108310.

References

[1] Y.Q. He, W. Fudickar, J.H. Tang, et al., J. Am. Chem. Soc. 142 (2020) 2601–2608.
[2] S. Martins, J.P.S. Farinha, C. Baleizao, et al., Chem. Commun. 50 (2014) 3317–3320.
[3] A. Atilgan, Y. Beldjoudi, J. Yu, et al., ACS Appl. Mater. Interfaces 14 (2022) 12596–12605.
[4] A. Atilgan, M.M. Cetin, J. Yu, et al., J. Am. Chem. Soc. 142 (2020) 18554–18564.
[5] A. Atilgan, T. Islamoglu, A.J. Howarth, et al., ACS Appl. Mater. Interfaces 9 (2017) 24555–24560.
[6] Q.Y. Wang, J. Liu, M. Cao, et al., Angew. Chem. Int. Ed. 61 (2022) e202207130.
[7] J. Hynek, M.K. Chahal, D.T. Payne, et al., Coord. Chem. Rev. 425 (2020) 213541.
[8] J.Y. Zeng, X.S. Wang, Y.D. Qi, et al., Angew. Chem. Int. Ed. 58 (2019) 5692–5696.
[9] Y. Zhang, J. Pang, J. Li, et al., Chem. Sci. 10 (2019) 8455–8460.
[10] D. Yan, E. Lin, F. Jin, et al., J. Mater. Chem. A 9 (2021) 27434–27441.
[11] J. Park, D. Feng, S. Yuan, et al., Angew. Chem. Int. Ed. 54 (2015) 430–435.
[12] J. Gao, J. Lu, B.Y. Li, et al., Chin. Chem. Lett. 33 (2022) 5132–5136.
[13] L.F. Chen, C.C. Hou, L.L. Zou, et al., Sci. Bull. 66 (2021) 170–178.
[14] S.J. Liu, C. Zhang, Y.D. Sun, et al., Coord. Chem. Rev. 413 (2020) 213266.
[15] K.L. Zhang, L. Wang, W.L. Cai, et al., Inorg. Chem. Front. 6 (2019) 955.
[16] H.S. Zheng, Y.Y. Hou, S. Li, et al., Chin. Chem. Lett. 33 (2022) 5013–5022.
[17] P. Cai, M. Xu, S.S. Meng, et al., Angew. Chem. Int. Ed. 60 (2021) 27258–27263.
[18] J. Pang, Z. Di, J.S. Qin, et al., J. Am. Chem. Soc. 142 (2020) 15020–15026.
[19] J. Pang, S. Yuan, J. Qin, et al., J. Am. Chem. Soc. 139 (2017) 16939–16945.
[20] J. Pang, S. Yuan, J. Qin, et al., J. Am. Chem. Soc. 140 (2018) 12328–12332.
[21] Y. Wang, M. Fu, S. Zhou, et al., Chem 8 (2022) 1–12.
[22] L. Yu, S. Ullah, H. Wang, et al., Angew. Chem. Int. Ed. 61 (2022) e202211359.
[23] Y. Tang, H. Wu, W. Cao, et al., Adv. Optical Mater. 9 (2020) 2001817.
[24] Q.Y. Pan, M.E. Sun, C. Zhang, et al., Chem. Commun. 57 (2021) 11394–11397.
[25] H. Zheng, Y. Hou, S. Li, et al., Chin. Chem. Lett. 33 (2022) 5013–5022.
[26] J.J. Huang, D. Zhao, G.J. Yin, Chin. J. Struct. Chem. 41 (2022) 2203030–2203039.
[27] C.R. Martin, K.C. Park, G.A. Leith, et al., J. Am. Chem. Soc. 144 (2022) 4457–4468.
[28] K.C. Park, C.R. Martin, G.A. Leith, et al., J. Am. Chem. Soc. 144 (2022) 16139–16149.
[29] M.F. Wang, Y. Mi, F.L. Hu, et al., J. Am. Chem. Soc. 142 (2020) 700–704.
[30] J. Pang, S. Yuan, J.S. Qin, et al., J. Am. Chem. Soc. 141 (2019) 3129–3136.
[31] X. Zhao, X. Bu, Q.G. Zhai, et al., J. Am. Chem. Soc. 137 (2015) 1396–1399.
[32] S.Y. Zhang, D. Fairen-Jimenez, M.J. Zaworotko, Angew. Chem. Int. Ed. 59 (2020) 17600–17606.
[33] T. He, B. Ni, S. Zhang, et al., Small 14 (2018) e1703929.
[34] Z.H. Long, D. Luo, K. Wu, et al., ACS Appl. Mater. Interfaces 13 (2021) 37102–37110.
[35] C. Wang, Z. Xie, K.E. deKrafft, et al., J. Am. Chem. Soc. 133 (2011) 13445–13454.
[36] M. Fujimura, S. Kusaka, A. Masuda, et al., Small 17 (2021) e2004351.
[37] M. Gupta, J.J. Vittal, Coord. Chem. Rev. 435 (2021) 213789.
[38] Z.Y. Li, Z.Q. Yao, R. Feng, et al., Chin. Chem. Lett. 32 (2021) 3095–3098.